

Static and dynamic aspects of an air-gap capacitor

Dominicus J IJntema and Harrie A C Tilmans

MESA Research Institute, University of Twente, P O Box 217, 7500 AE Enschede (Netherlands)

(Received September 23, 1991, in revised form March 10, 1992, accepted June 16, 1992)

Abstract

This paper deals with the theory of an air-gap capacitor used as a micromechanical resonator. Both static and dynamic aspects are discussed. A single-element approach for the electrostatic excitation and capacitive detection of the vibrational motion of the resonators is described. The non-linear character of the electrostatic force is accounted for in the static analysis. The behaviour of the air-gap capacitor is modelled as a lumped spring-mass system and its limitations are discussed. Also an equivalent electrical one-port network is derived, which can be used in a circuit simulation to account for the mechanical behaviour of the resonator. The results obtained from the spring-mass system are compared with the results obtained from a more elaborate numerical analysis of the air-gap capacitor. The lumped spring-mass system is adequate for modelling the air-gap capacitor.

Introduction

The air-gap capacitor consists of two electrodes separated by a gap. The gap can be air (or any other gas) or vacuum. The structure forms a (micro)mechanical resonator, which can be used as the sensing element in mechanical sensors [1, 2]. In this paper only flexurally vibrating elements are discussed. One electrode is formed by the vibrating element, e.g., a beam, and the other electrode by a stationary surface in close proximity to the vibrating element. A schematic cross section of the structure is shown in Fig 1.

The structure is excited by means of the electrostatic force between the capacitor plates. The vibrational motion is detected as a change of the capacitance caused by the fluctuating gap spacing. Electrostatic excitation/capacitive detection was first described by Nathanson *et al* in 1967 [3] and

has been used by several authors since then [4–6]. Here, a two-terminal device is described, where a single element is used for both the excitation and detection of the vibration [5, 7, 8]. The structure can be modelled as an electrical one-port network. This is in contrast to the two-port approach, where separate elements are used for the excitation and detection of the motion [4, 6].

In this paper, the effect of the static deflection caused by the d.c. polarization voltage is included in the analysis of the behaviour of a clamped-clamped prismatic beam. The pull-in voltage and the resonance frequency of the air-gap capacitor and the modal capacitance of the equivalent electrical network are computed using numerical methods. Guidelines are given to derive a lumped spring-mass system for a given air-gap capacitor.

Principle of operation

The air-gap capacitor typically consists of a clamped-clamped beam with a top drive electrode extending from $x = x_1$ to $x = x_2$, see Fig 1. The bottom electrode is formed by a stationary surface. The a.c. drive voltage $u(t)$ is superimposed onto a d.c. polarization voltage V_P to avoid excitation at twice the drive frequency [3]. The vibrational motion will change the gap spacing and therefore also the capacitance. Because of the

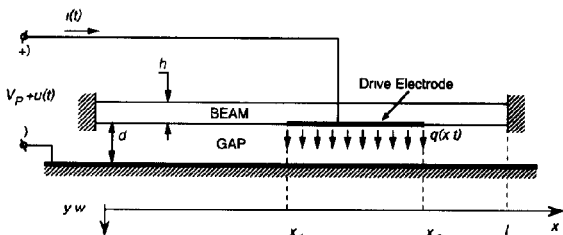


Fig 1 Sketch of an electrostatically excited and capacitively detected beam (air-gap capacitor), driven by means of a single element

changing capacitance, an a c current will flow through the air-gap capacitor. The a c current is a measure of the amplitude of the vibration. The polarization voltage V_P across both electrodes will cause an electrostatic force between the top electrode and the bottom electrode which is inversely proportional to the square of the gap spacing. Due to the non-linear behaviour of the electrostatic force, there is a possibility of instability, i.e., collapse of the structure. An axial strain applied to the beam will change the resonance frequency, and in this way the air-gap capacitor can be used as a strain-sensing element [2]. Typical dimensions of a micromechanical air-gap resonator are gap spacing = 1–2 μm , length = 100–500 μm , width = 10–100 μm and thickness = 1–3 μm .

Theoretical model

The differential equation of motion governing the deflection $W(x, t)$ of a prismatic beam with a rectangular cross section, subjected to an axial tensile load N and a transverse electrostatic drive load $q(x, t)$ can be expressed as

$$E'I \frac{\partial^4 W(x, t)}{\partial x^4} - N \frac{\partial^2 W(x, t)}{\partial x^2} + qb \frac{\partial^2 W(x, t)}{\partial t^2} + c \frac{\partial W(x, t)}{\partial t} = q(x, t) \quad (1)$$

where E' , I , q and c are the effective Young's modulus, second moment of inertia, specific mass and the viscous drag parameter, respectively, and b , h , x and t are the width and thickness of the beam, position along the beam length and time, respectively. For wide beams ($b > 5h$) the effective Young's modulus equals $E/(1 - \nu^2)$ [9], where E and ν are Young's modulus and Poisson's ratio, respectively. The air-gap capacitor is excited by applying an a c drive voltage $u(t)$ superimposed on a d c polarization voltage V_P [3–5, 7]. The polarization voltage V_P causes a static deflection $y_{\text{stat}}(x)$ of the beam. The overall deflection $W(x, t)$ can be written as a superposition of the static deflection $y_{\text{stat}}(x)$ and the dynamic deflection $w(x, t)$. $W(x, t) = y_{\text{stat}}(x) + w(x, t)$. Assuming the direction of the electric field vector to be perpendicular to the x -axis along the entire beam length (Fig. 1) and for $w(x, t) \ll d - y_{\text{stat}}(x)$ and $u(t)^2 \ll V_P^2$, the electrostatic load can be expressed as a superposi-

tion of a static load $q_{d c}(x)$ and a dynamic load $q_{a c}(x)$

$$\begin{aligned} q(x, t) &= \frac{1}{2} \frac{\epsilon_0 \epsilon_r b [V_P + u(t)]^2}{[d - y_{\text{stat}}(x) - w(x, t)]^2} \\ &\approx \frac{1}{2} \frac{\epsilon_0 \epsilon_r b V_P^2}{[d - y_{\text{stat}}(x)]^2} + \frac{\epsilon_0 \epsilon_r b u(t) V_P}{[d - y_{\text{stat}}(x)]^2} \\ &\equiv q_{d c}(x) + q_{a c}(x, t) \end{aligned} \quad (2)$$

where ϵ_0 , ϵ_r and d are the dielectric constant of vacuum, the relative dielectric constant of the gap medium and the zero-voltage gap spacing, respectively.

Static behaviour

The attractive electrostatic force $q_{d c}(x)$ caused by the polarization voltage V_P is inversely proportional to the square of the gap spacing $d - y_{\text{stat}}(x)$ (eqn (2)). An increase of the deflection of the beam results in a decrease of the gap spacing and thus in an increase of the electrostatic force. If V_P exceeds the so-called pull-in voltage V_{PI} , the deflection does not reach an equilibrium position and will continue to increase until physical contact is made with the stationary bottom electrode. The system is mechanically unstable [3]. For polarization voltages smaller than V_{PI} , the deflection $y_{\text{stat}}(x)$ will reach an equilibrium position and the electrostatic force balances the restoring force caused by the stiffness of the beam. The static deflection $y_{\text{stat}}(x)$ can be found by solving the non-linear differential eqn (1), thereby setting the time derivatives equal to zero. An analytical closed-form solution of the deflection curve $y_{\text{stat}}(x)$ cannot be found, instead an iterative numerical procedure can be used. The iterative solution process can be expressed as

$$\begin{aligned} E'I \frac{d^4 y_n(x)}{dx^4} &= \frac{1}{2} \frac{\epsilon_0 \epsilon_r b V_P^2}{[d - y_{n-1}(x)]^2} \\ &\quad + N \frac{d^2 y_{n-1}(x)}{dx^2} \quad n = 2, 3, 4, \\ y_1(x) &= 0 \\ \frac{d^2 y_1(x)}{dx^2} &= 0 \end{aligned} \quad (3)$$

where $y_n(x)$ is the n th iteration of the static deflection, satisfying the boundary conditions of the beam. For the numerical computations, the beam is divided into a finite number of length intervals

The fourth to the first derivatives and the displacement at every point in the interval are computed using the backward Euler method [10] For polarization voltages V_P smaller than the pull-in voltage V_{PI} , the algorithm of eqn (3) will converge to the equilibrium static deflection of the beam For polarization voltages exceeding the pull-in voltage, the static deflection will continue to increase and finally equals the gap distance d For small axial loads N the algorithm described by eqn (3) works properly For moderate axial loads, however, only a fraction of the change in y_n and $y_n^{(2)}$ between two iterations should be used to ensure convergence For large axial loads, the clamped-clamped beam can be modelled as a string, i.e., ignoring the term with the fourth derivative in eqn (1) The algorithm described in eqn (3) can now be written as

$$N \frac{d^2 y_n(x)}{dx^2} = -\frac{1}{2} \frac{\epsilon_0 \epsilon_r b V_P^2}{[d - y_{n-1}(x)]^2} \quad n = 2, 3, 4, \quad (4)$$

$$y_1(x) = 0$$

The numerical solution methods described above can be used for polarization voltages close to V_{PI} In normal operation of the air-gap capacitor applied as a resonator, the polarization voltage will be much smaller than the pull-in voltage, resulting in a deflection of the beam that is small compared to the gap spacing In this case, the load given by eqn (2) can be linearized, and a set of first-order differential equations is obtained, which can be solved numerically with known algorithms [10] Other methods based on minimum-energy principles, where an approximate shape function for the deflection of the beam is assumed, can also be used [11]

Dynamic behaviour

The steady-state solution of eqn (1), for a beam with length l , driven by a harmonic driving load $q_{ac}(x, t) = q_{ac}(x) \exp(j\omega t)$ can be obtained using a modal analysis [8, 12, 13]

$w(x, t)$

$$= \sum_{n=1}^{\infty} \frac{\phi_n(x) \int_{x_1}^{x_2} \phi_n(x) q_{ac}(x) dx}{\omega_n^2 M_n \left[1 + \frac{1}{Q_n} \left(\frac{j\omega}{\omega_n} \right) + \left(\frac{j\omega}{\omega_n} \right)^2 \right]} \exp(j\omega t) \quad (5)$$

where

$$M_n = \rho b h \int_0^l \phi_n(x)^2 dx \quad (\text{generalized mass})$$

and $\phi_n(x)$ and ω_n are the mode shape function and the natural frequency of the n th mode, respectively, which can be found by solving the eigenvalue problem associated with eqn (1) [14], and Q_n is the quality factor of the n th mode Optimal excitation of a particular mode is achieved when the integral in the numerator is maximal On the other hand, suppression of a certain mode is achieved by making the integral very small or, better, zero This can be done by a proper choice of the electrode configuration To excite the fundamental mode ($n = 1$), one can take a symmetric electrode configuration with respect to the centre of the beam In this way all the asymmetric modes will be suppressed Theoretically, it is possible to excite the fundamental symmetric mode with a lower efficiency compared to the optimal excitation of the fundamental mode, meanwhile suppressing the second mode (asymmetric), the third mode (symmetric), the fourth mode (asymmetric) and all higher-order asymmetric modes This is achieved by designing a symmetric electrode configuration with respect to the centre of the beam in such a way that the integral in the numerator of eqn (5) equals zero for the third mode

To derive an electrical one-port network of the air-gap capacitor of Fig 1, the admittance seen at the electrical terminals is derived [8] The small signal detection current $i(t)$ flowing into the port is given by (for $u(t) \ll V_P$)

$$i(t) \approx C_0 \frac{du(t)}{dt} + V_P \frac{dC(t)}{dt} \quad (6)$$

where C_0 is the static capacitance, given by

$$C_0 = \epsilon_0 \epsilon_r b \int_{x_1}^{x_2} \frac{dx}{d - y_{stat}(x)} \quad (7)$$

and $C(t)$ is the momentary capacitance For vibrational amplitudes that are small compared to the gap spacing, the time derivative of the momentary

capacitance is given by

$$\begin{aligned} \frac{dC(t)}{dt} &= \epsilon_0 \epsilon_r b \frac{d}{dt} \int_{x_1}^{x_2} \frac{dx}{d - y_{\text{stat}}(x) - w(x, t)} \\ &\approx j\omega \epsilon_0 \epsilon_r b \int_{x_1}^{x_2} \frac{w(x) dx}{[d - y_{\text{stat}}(x)]^2} \end{aligned} \quad (8)$$

where $w(x)$ is the amplitude of the vibration, $w(x, t) = w(x) \exp(j\omega t)$. The approximation in eqn (8) applies for $w(x) \ll d - y_{\text{stat}}(x)$. Combining eqns (2), (5), (6), (7) and (8) yields an expression for the admittance $Y(j\omega)$ of the air-gap capacitor

$$\begin{aligned} Y(j\omega) &\equiv \frac{i}{u} = j\omega C_0 \\ &+ \sum_{n=1}^{\infty} j\omega \frac{(\epsilon_0 \epsilon_r b V_P)^2}{\omega_n^2 M_n \left[1 + \frac{1}{Q_n} \left(\frac{j\omega}{\omega_n} \right) + \left(\frac{j\omega}{\omega_n} \right)^2 \right]} \\ &\times \left[\int_{x_1}^{x_2} \frac{\phi_n(x) dx}{[d - y_{\text{stat}}(x)]^2} \right]^2 \end{aligned} \quad (9)$$

The expression for the admittance of the air-gap capacitor given by eqn (9) can be represented by the one-port network shown in Fig 2 [8, 13]. This equivalent electrical network can subsequently be used in a circuit simulation, e.g., SPICE, as a convenient way to account for the mechanical behaviour of the resonator. The static capacitance

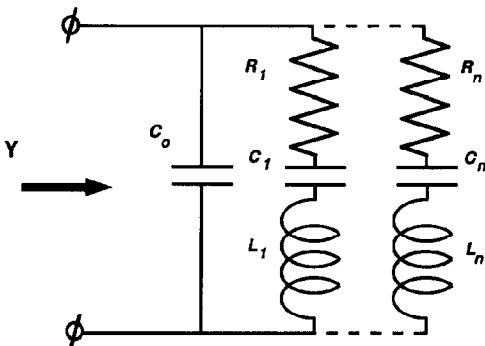


Fig 2 Equivalent electrical one-port network of the air-gap capacitor shown in Fig 1

C_0 is given by eqn (7). The dynamic component values of the electrical network are given by

$$C_n = \frac{(\epsilon_0 \epsilon_r b V_P)^2}{\omega_n^2 M_n} \left[\int_{x_1}^{x_2} \frac{\phi_n(x) dx}{[d - y_{\text{stat}}(x)]^2} \right]^2 \quad (10)$$

$$L_n = \frac{1}{\omega_n^2 C_n} \quad (11)$$

and

$$R_n = \frac{1}{Q_n} \left(\frac{L_n}{C_n} \right)^{1/2} \quad (12)$$

Mechanical instability, caused by polarization voltages exceeding V_{PI} , has already been discussed in the previous Section. Another effect of the polarization voltage is the lowering of the natural frequency of the air-gap capacitor due to the gradient in the transverse electrostatic force, which varies with the polarization voltage [3]. A good approximation for the resonance frequency can be found from an analysis based on Rayleigh's energy method [12]. Besides the contribution to the potential energy due to bending and axial deformation of the beam, an additional term $E_{\text{load}}(V_P)$, representing the change in energy of the electric field in the gap due to the vibration, must be included. Using a first-order approximation, this term can be expressed as

$$\begin{aligned} E_{\text{load}}(V_P) &\approx - \int_{x_1}^{x_2} \int_0^{\tilde{w}(x)} \frac{\partial q(x, t)}{\partial w(x, t)} \Big|_{w(x, t)=0} \\ &\times w(x) dw(x) dx \\ &= - \frac{1}{2} \int_{x_1}^{x_2} \frac{\partial q(x, t)}{\partial w(x, t)} \Big|_{w(x, t)=0} \tilde{w}^2(x) dx \\ &\approx - \frac{1}{2} \int_{x_1}^{x_2} \frac{\epsilon_0 \epsilon_r b V_P^2}{[d - y_{\text{stat}}(x)]^3} \tilde{w}^2(x) dx \end{aligned} \quad (13)$$

where $\tilde{w}(x)$ is the assumed shape of the particular mode and $q(x, t)$ is given by eqn (2). The last approximation in eqn (13) applies for $u(t) \ll V_P$ and $w(x) \ll d - y_{\text{stat}}(x)$. The angular resonance frequency $\omega_n(N, V_P)$ of mode n as a function of the axial load N and the polarization voltage V_P can

be expressed as

$$\omega_n^2(N, V_P) = \frac{EI \int_0^l \left(\frac{d^2 \tilde{w}(x)}{dx^2} \right)^2 dx + N \int_0^l \left(\frac{d \tilde{w}(x)}{dx} \right)^2 dx - \epsilon_0 \epsilon_r b V_P^2 \int_{x_1}^{x_2} \frac{\tilde{w}^2(x)}{[d - y_{\text{stat}}(x)]^3} dx}{\rho b h \int_0^l \tilde{w}^2(x) dx} \quad (14)$$

The first two terms in the numerator represent the potential energy due to bending and axial deformation of the beam, respectively. The last term of the numerator represents the change in potential energy due to work done by the electrostatic force. This term makes the resonance frequency dependent on the polarization voltage V_P . At the pull-in voltage, the fundamental frequency ($n = 1$) equals zero. This behaviour is similar to the buckling phenomenon [14]. The resonance frequency of the higher-order modes will not equal zero at the pull-in voltage.

To indicate the dependence of the angular resonance frequency of the fundamental mode ($n = 1$) ω_1 on the applied axial strain $\varepsilon = N/(Ebh)$ and on the polarization voltage V_P , the angular resonance frequency of the fundamental mode can conveniently be written as

$$\omega_1^2(\varepsilon, V_P) = \omega_1^2(\varepsilon) + \frac{E_{\text{load}}(V_{PI})}{\frac{1}{2} \rho b h \int_0^l \tilde{w}^2(x) dx} \quad (15)$$

where

$$\omega_1^2(\varepsilon) = \omega_{10}^2 \left[1 + 0.295\varepsilon(1 - \nu^2) \left(\frac{l}{h} \right)^2 \right] \quad (16)$$

and ω_{10} is the angular resonance frequency of the fundamental mode for zero applied strain. The expression above (eqn (16)) is found from an analysis based on Rayleigh's energy method, where the mode shape for zero applied axial load is taken as the approximate shape function [2].

Spring-mass model

Because of the complexity of the model of the air-gap capacitor, which makes it unsuitable for quick design calculations, it would be attractive to have a simple model to predict the static and dynamic behaviour of the resonator with sufficient

accuracy. A lumped spring-mass system, see Fig 3, provides such a model [3], but the accuracy of the model has never been verified. The lumped spring-mass system is dimensioned in such a way that the static and dynamic behaviours of the spring-mass system resemble the static and dynamic behaviours of the air-gap capacitor in a narrow frequency regime around the fundamental mode. Also, the spring-mass system has to be dimensioned without the necessity for difficult calculations. The zero-voltage gap spacing d and the electrode area $A = (x_2 - x_1)b$ are chosen to be the same for both systems. An appropriate choice for the spring constant K_0 of the spring-mass system would be the static spring constant seen at the centre of the beam for zero applied axial load. For a drive electrode with a uniform width, the spring constant K_0 could be defined as the spring constant of a beam subjected to uniform load q_0

$$K_0 = \frac{\int_{x_1}^{x_2} q_0 dx}{y_{\text{stat}} \left(\frac{l}{2} \right) \Big|_{q_0}} \quad (17)$$

For a clamped-clamped beam with the drive electrode extending along the entire beam length, K_0 is given by $K_0 = 384E'I/l^3$. An additional term K_ε given by eqn (20) is added to include the effect of the axial strain. The overall spring constant K is given by $K = K_0 + K_\varepsilon$, see also Fig 3.

The mass of the spring-mass system is chosen in such a way that its resonance frequency equals the fundamental resonance frequency of the air-gap capacitor with zero applied polarization voltage, as given by eqn (16). For the lumped spring-mass system the angular resonance frequency $\omega_1^{\text{sm}}(\varepsilon)$, with zero applied polarization voltage, is given by

$$\omega_1^{\text{sm}}(\varepsilon) = \left(\frac{K}{M} \right)^{1/2} = \left(\frac{K_0}{M} + \frac{K_\varepsilon}{M} \right)^{1/2} \quad (18)$$

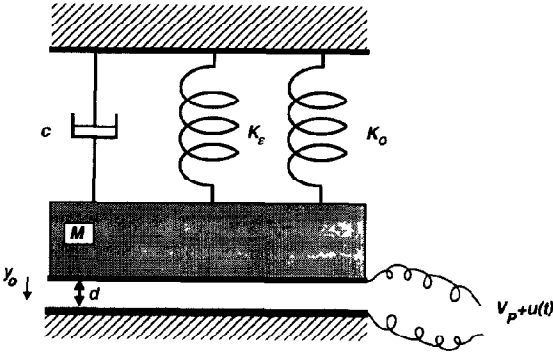


Fig 3 Sketch of the equivalent spring-mass system that is used as a model for the air-gap capacitor and can be used for quick design calculations. K_0 is the static spring constant seen at the centre of the beam for zero applied axial load. An additional spring constant K_e is added to include the effect of the axial strain.

Combining eqns (16) and (18) for $\varepsilon = 0$ yields the mass of the spring-mass system

$$M = K_0/\omega_{10}^2 \quad (19)$$

The spring constant K_e is found by combining eqns (16), (18) and (19)

$$K_e = K_0 0.295\varepsilon(1 - v^2) \left(\frac{l}{h}\right)^2 \quad (20)$$

The angular resonance frequency of the spring-mass system $\omega_1^{\text{sm}}(\varepsilon, V_p)$ as a function of the axial strain (applied to the air-gap capacitor) and the polarization voltage can be expressed as [3]

$$\omega_1^{\text{sm}}(\varepsilon, V_p) = \omega_1^{\text{sm}}(\varepsilon) \left(3 - 2 \frac{d}{d - y_0(V_p)}\right)^{1/2} \quad (21)$$

where $y_0(V_p)$ is the static displacement of the spring-mass system caused by the polarization voltage V_p . $y_0(V_p)$ can be found by solving the following cubic equation resulting from force equilibrium [3]

$$K y_0 = \frac{1}{2} \frac{\varepsilon_0 \varepsilon_r A V_p^2}{[d - y_0]^2} \Rightarrow y_0 = y_0(V_p) \quad (22)$$

The viscous drag parameter c of the spring-mass system can be calculated from the quality factor Q_1 of the air-gap capacitor by

$$c = \frac{M \omega_1^{\text{sm}}(\varepsilon, V_p)}{Q_1} \quad (23)$$

An expression for the pull-in voltage $V_{\text{PI}}^{\text{sm}}$ of the spring-mass system can easily be derived by setting the derivative of the net force acting on the spring-

mass system equal to zero [3]. Combining this result with the spring constant $K = K_0 + K_e$ of a clamped-clamped beam with the drive electrode extending along the entire beam length gives an approximate expression for the pull-in voltage of the beam

$$\begin{aligned} V_{\text{PI}}^{\text{sm}} &= \left(\frac{8}{27} \frac{K d^3}{\varepsilon_0 \varepsilon_r A}\right)^{1/2} \\ &= 10.7 \left\{ \frac{E' I d^3}{\varepsilon_0 \varepsilon_r A l^3} \left[1 + 0.295\varepsilon(1 - v^2) \left(\frac{l}{h}\right)^2 \right] \right\}^{1/2} \end{aligned} \quad (24)$$

The admittance seen at the electrical terminals of the spring-mass system can be derived in a similar way as for the air-gap capacitor. The static capacitance C_0^{sm} and modal capacitance C_1^{sm} of the spring-mass system are given by

$$C_0^{\text{sm}} = \frac{\varepsilon_0 \varepsilon_r A}{d - y_0(V_p)} \quad (25)$$

and

$$C_1^{\text{sm}} = \frac{V_p^2 (C_0^{\text{sm}})^2}{M \omega_1^{\text{sm}}(\varepsilon, V_p)^2 [d - y_0(V_p)]^2} \quad (26)$$

Results

To have some idea about the accuracy of the results obtained from the spring-mass system, a few examples are presented. The equivalent spring-mass system is dimensioned with the guidelines given in the last paragraph. First the pull-in voltage obtained from the model of the air-gap capacitor is compared with the pull-in voltage obtained from the spring-mass model.

The pull-in voltage V_{PI} of the air-gap capacitor is computed with the algorithm described by eqns (3) and (4). The pull-in voltage $V_{\text{PI}}^{\text{sm}}$ of the equivalent spring-mass system is computed from eqn (24). The results of the computation of the pull-in voltages for different beam dimensions are given in Table 1. It turns out that the estimated pull-in voltage $V_{\text{PI}}^{\text{sm}}$ is roughly 10% lower than the actual pull-in voltage V_{PI} computed for an air-gap capacitor with the electrode extending along the entire beam length and for small axial strains. It can be shown that for higher strain levels and/or an electrode not extending along the entire beam length, the estimation will be more accurate.

TABLE 1 Pull-in voltage and resonance frequency of the air-gap capacitor and the equivalent spring-mass model for various dimensions and axial strains ($E = 175$ GPa, $\rho = 2330$ kg m $^{-3}$, $\nu = 0.3$ and $\epsilon_r = 1$)

Length (μm)	Width (μm)	Thickness (μm)	Gap (μm)	Strain	V_{PI} (V) beam	V_{PI}^{sm} (V) lumped
500	100	1.5	1.0	0.0	3.8	3.4
500	100	1.5	5.0	0.0	42	38
100	100	1.5	1.0	0.0	94	85
500	100	1.5	1.0	10^{-5}	4.3	3.9
500	100	1.5	1.0	10^{-2}	58	61
500	100	6.0	1.0	0.0	30	27

The modal capacitance C_1 and the angular resonance frequency $\omega_1(\epsilon, V_P)$ of the fundamental mode as a function of the applied axial strain and the polarization voltage are computed for the air-gap capacitor and compared with the modal capacitance C_1^{sm} and the angular resonance frequency $\omega_1^{sm}(\epsilon, V_P)$ obtained from the spring-mass system. To calculate the modal capacitance C_1 and the resonance frequency $\omega_1(\epsilon, V_P)$, first the static deflection $y_{stat}(x)$ is computed from eqns (3) or (4). An eighth-order polynomial of the static deflection curve of the beam is generated for a given polarization voltage. The polynomial fit of the static deflection is used in eqns (10) and (13) to obtain the modal capacitance C_1 and $E_{load}(V_P)$, respectively. For $\phi_1(x)$ and $\tilde{w}(x)$, the mode shape of a clamped-clamped beam with an axial strain is used in eqns (10) and (13) [2]. For large axial strains ($\epsilon = 10^{-2}$), a sine function is used as the approximated mode-shape function. The angular resonance frequency is computed numerically from eqn (15). To calculate the modal capacitance C_1^{sm} and the angular resonance frequency $\omega_1^{sm}(\epsilon, V_P)$, the static deflection $y_0(V_P)$ of the spring-mass system has to be calculated. A closed-form expression of the static deflection can be found by using a first-order Taylor series expansion for the solution of eqn (22), which results in

$$y_0(V_P) \approx \frac{1}{2} \frac{\epsilon_0 \epsilon_r A V_P^2 d}{K d^3 - \epsilon_0 \epsilon_r A V_P^2} \quad (27)$$

For polarization voltages up to $0.8 V_{PI}^{sm}$ the error in the static displacement is less than 5%. For a polarization voltage of $0.9 V_{PI}^{sm}$ the error is 10%. In practical situations, where the polarization voltage is much smaller than the pull-in voltage, eqn (27)

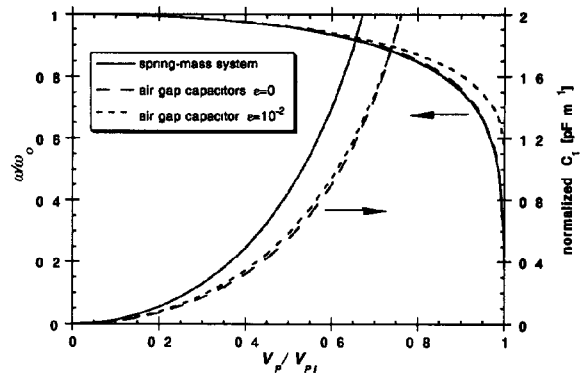


Fig 4 The normalized modal capacitance ($C_1^* d/bI$, $C_1^{sm} d/A$) and the normalized angular resonance frequency ($\omega_1(\epsilon, V_P)/\omega_1(\epsilon, 0)$, $\omega_1^{sm}(\epsilon, V_P)/\omega_1^{sm}(\epsilon, 0)$) vs the normalized polarization voltage (V_P/V_{PI} , V_P/V_{PI}^{sm}) of the air-gap capacitor with various dimensions and of the equivalent spring-mass system. The curves of the air-gap capacitors with zero or small applied axial strains all more or less coincide.

will provide a good approximation of the static displacement of the spring-mass system. Because the static deflection $y_0(V_P)$ given by eqn (27) is not accurate for polarization voltages close to the pull-in voltage V_{PI}^{sm} , eqn (22) is solved numerically.

Figure 4 shows the normalized modal capacitance of the air-gap capacitor ($C_1^* d/bI$) and the normalized angular resonance frequency of the air-gap capacitor ($\omega_1(\epsilon, V_P)/\omega_1(\epsilon, 0)$) as a function of the normalized polarization voltage for beams of various dimensions and different applied axial strains (see also Table 1). The angular resonance frequency is normalized to the angular resonance frequency with zero applied polarization voltage. The curves of the beams with zero and small applied strains all coincide. Figure 4 also shows the normalized modal capacitance ($C_1^{sm} d/A$) and the normalized angular resonance frequency ($\omega_1^{sm}(\epsilon, V_P)/\omega_1^{sm}(\epsilon, 0)$) calculated from the equivalent spring-mass model. The modal capacitance C_1^{sm} found with the help of the spring-mass system is roughly a factor 1.5 larger than the modal capacitance C_1 of the air-gap capacitor. The resonance frequencies as a function of the polarization voltage of the air-gap capacitor and the spring-mass system are approximately equal. The modal capacitance C_1^{sm} found from the spring-mass model can be used, after correction with a factor 1.5, in the electrical equivalent circuit of the one-port resonator.

Conclusions

A model of the electrostatically driven and capacitively detected resonator based on a single-element approach is presented, thereby including in the static behaviour the non-linear effects of the electrostatic force. Guidelines are given to dimension a lumped spring-mass system for a given air-gap capacitor, without the need for tedious calculations. For engineering purposes, the electrostatically driven resonator can be described sufficiently accurately by a lumped spring-mass system. The pull-in voltage computed from the spring-mass system is roughly 10% lower than the value computed for the air-gap capacitor. The dependence of the resonance frequency on the normalized polarization voltage is approximately the same for both the spring-mass system and for the air-gap capacitor. The equivalent electrical network can be used in circuit simulations to account for the resonator behaviour in a narrow frequency range around the fundamental frequency. The electrical network can be dimensioned rapidly with the help of this lumped spring-mass system.

Acknowledgement

The authors would like to thank Professor Jan Fluitman for helpful discussions and suggestions.

References

- 1 R T Howe, Resonant microsensors, *Proc 4th Int Conf Solid-State Sensors and Actuators (Transducers '87)*, Tokyo, Japan, June 2-5, 1987, pp 843-848
- 2 H A C Tilmans, M Elwenspoek and J H J Fluitman, Micro resonant force gauges, *Sensors and Actuators A*, 30 (1992) 35-53
- 3 H C Nathanson, W E Newel, R A Wickstrom and J R Davis, Jr, The resonant gate transistor, *IEEE Trans Electron Devices*, ED-14 (1967) 117-133
- 4 R T Howe and R S Muller, Resonant-microbridge vapor sensor, *IEEE Trans Electron Devices*, ED-33 (1986) 499-506
- 5 M W Putty, S C Chang, R T Howe, A L Robinson and K D Wise, One-port active polysilicon resonant microstructures, *Proc IEEE MEMS '89 Workshop, Salt Lake City, UT, USA, 1989*, pp 60-65
- 6 C Linder, E Zimmerman and N F de Rooij, Capacitive polysilicon resonator with MOS detection circuit, *Sensors and Actuators A*, 25-27 (1991) 591-595
- 7 M W Putty, Polysilicon resonant microstructures, *Master's Thesis*, University of Michigan, 1988
- 8 H A C Tilmans, D J IJntema and J H J Fluitman, Single element excitation and detection of (micro-)mechanical resonators, *Proc 6th Int Conf Solid-State Sensors and Actuators (Transducers '91)*, San Francisco, USA, June 24-27, 1991, pp 533-537
- 9 S P Timoshenko and S Woinowski-Kreiger, *Theory of Plates and Shells*, McGraw-Hill, New York, 2nd edn, 1970, p 5

- 10 W H Press, B P Flannery, S A Teukolsky and W T Vetterling, *Numerical Recipes, The Art of Scientific Computing*, Cambridge University Press, Cambridge, 1987
- 11 H A C Tilmans and R Legtenberg, Electrostatically driven vacuum encapsulated polysilicon resonators. Part II Performance, submitted to *Euroensors VI, San Sebastian, Spain, Sept 30-Oct 2, 1992*
- 12 L Meirovitch, *Elements of Vibration Analysis*, McGraw-Hill, New York, 1975, Ch 5, pp 190-231
- 13 H A C Tilmans, Single element excitation and detection of (micro-)mechanical resonators—theory and experiments, to be published
- 14 S Bouwstra and B Geijselaers, On the resonance frequencies of microbridges, *Proc 6th Int Conf Solid-State Sensors and Actuators (Transducers '91)*, San Francisco, USA, June 24-27, 1991, pp 538-542

Biographies

Dominicus J IJntema was born in 1966 in Joure, The Netherlands. He received a M S degree in electrical engineering from the University of Twente in March 1991. His master's project dealt with a 'differential resonator design using electrostatically excited resonant gauges'. In May 1991 he became a research engineer at the MESA Research Institute of the University of Twente, The Netherlands, where he was working on a micromachined eye-pressure regulator for glaucoma patients. Currently he is working at Philips National Research Laboratory in Eindhoven.

Harrie A C Tilmans was born in 1957 in Elsloo, The Netherlands. He received his M S degree in electrical engineering from the University of Twente, Enschede, The Netherlands, in May 1984. In June 1984 he became a temporary research associate at the University of Twente, where he worked on the development of a resonating force sensor. In April 1985 he joined the faculty of Electrical and Computer Engineering of Boston University, Boston, USA, as a visiting instructor. In August 1986 he became a research assistant at the Wisconsin Center for Applied Microelectronics at the University of Wisconsin, Madison, WI, USA, where he worked on the development of a CMOS process and on the development of polysilicon micromechanical resonators. In August 1988 he returned to the The Netherlands, where he joined the MESA Research Institute of the University of Twente as a research associate. Currently, he is preparing for his Ph D thesis, on the subject of micro-mechanical sensors using encapsulated resonant strain gauges, which will be due in January 1993.